DOI 10.1007/s11182-018-1378-6

Russian Physics Journal, Vol. 61, No. 1, May, 2018 (Russian Original No. 1, January, 2018)

INFLUENCE OF MAGNETICALLY CONJUGATE FRAGMENTS OF AURORAL EMISSION IMAGES ON THE ACCURACY OF DETERMINING E_{av} OF PRECIPITATING ELECTRONS

M. A. Banshchikova,[1] I. N. Chuvashov,[1] A. K. Kuzmin,[2] and G. M. Kruchenitskii[3]

UDC 523.59: 551.594.5: 621.371: 550.388.2

Results of magnetic conjugation of image fragments of auroral emissions at different altitudes along the magnetic field lines and preliminary results of evaluation of their influence on the accuracy of remote mapping of energy characteristics of precipitating electrons are presented. The results are obtained using the code of tracing being an integral part of the software Vector M intended for calculation of accompanying, geophysical, and astronomical information for the center of mass of a space vehicle (SV) and remote observation of aurora by means of Aurovisor-VIS/MP imager onboard the SV Meteor-MP to be launched.

Keywords: Aurovizor-VIS/MP, SV Meteor-MP, tracing along a geomagnetic field line, conjugation of image fragments, auroral emissions.

INTRODUCTION

Dynamic charged particle precipitations in auroral oval and polar cap during substorms and their electrodynamic consequences (gradients of electron concentration, field aligned currents, and gradients of transverse conductances) engender inhomogeneities of the Earth's ionospheric plasma. Direct indicators of particle precipitation in different MLT sectors (under the MLT we hereinafter understand the magnetic local time in the CGM (Corrected Geomagnetic Coordinates) [1]) in different stages of magnetospheric substorms are different structures of the auroral emissions with different spatial scales. The intensity distributions of concrete auroral emissions display at atmosphere-ionosphere screen the energy characteristics of precipitating particles with different degrees of accuracy [2–6]. Images of these distributions can be recorded both from the Earth's surface and from an orbit [7]. Radio signals from the transmitter placed onboard a navigation satellite undergo scintillations when passing through the perturbed ionosphere to the receiver on the Earth surface. A correlation analysis of scintillations of signals at different frequencies from navigation satellites GPS, GLONASS, etc. demonstrates their very complicated relationship with electrodynamic online parameters of the polar ionosphere depending on the structures of precipitating charged particles that finally are displayed in the gradients of intensity emissions in small-scale auroral arcs and polar cap spots observed from the Earth's surface [8] and-or from SV orbits.

The present work is devoted an analysis of images of auroral emissions [9] recorded at the Amundsen–Scott Station (Antarctica) located on the South Pole with coordinates (–90°, 0°) simultaneously with detection and ranging and measurements of scintillations of signals from navigation satellites. Two emissions were observed at the Station: at λ630.0 nm ($h \approx 200$ km) and λ557.7 nm ($h \approx 115$–120 km).

[1]National Research Tomsk State University, Tomsk, Russia, e-mail: mba-tomsk@mail.ru; chuvashovin@gmail.com; [2]Space Research Institute of the Russian Academy of Sciences, Moscow, Russia, e-mail: 2017alkkuzmin@gmail.com; [3]Central Aerological Observatory of the Russian Federal Hydrometeorology and Environmental Monitoring Service, Moscow Institute of Physics and Technology (State University), Moscow, Russia, e-mail: omd@cao-rhms.ru. Translated from Izvestiya Vysshikh Uchebnykh Zavedenii, Fizika, No. 1, pp. 132–137, January, 2018. Original article submitted July 28, 2017.

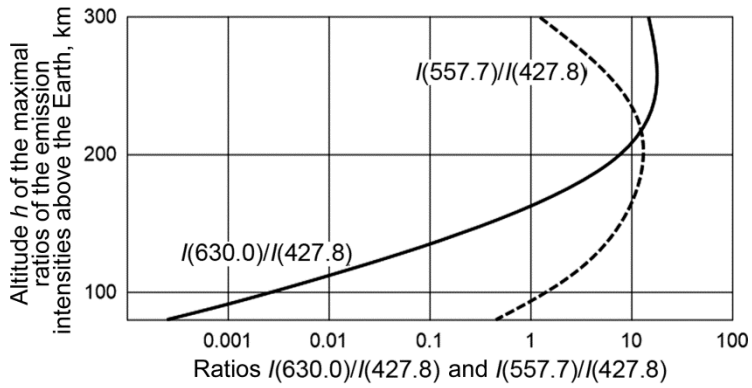

Fig. 1. Dependences of the ratios of the emission intensities $I(630.0/I(427.8)$ and $I(557.7/I(427.8)$ on the altitude h [2].

In connection with upcoming orbital experiment with a helio geophysical complex of equipment placed onboard the SV Meteor-MP [10] aimed at investigation of processes proceeding in the magnetosphere-ionosphere and their influence on signal propagation in the ionosphere [8], we have tried to estimate the influence of conjugation (along magnetic field line) of image fragments of auroral emissions at different altitudes on the accuracy of determining ratios of the intensities of concrete emissions. In the auroral zone, auroral precipitating electrons and protons observed along the magnetic field lines (m.f.l.) deviated from the vertical to the Earth at angles exceeding 10°. Therefore, it is physically correctly to analyze the intensity distributions in geometrically coaxial images of emissions observed at different altitudes taking into account the conjugation of image fragments along the m.f.l.

1. RELATIONSHIP OF THE RATIOS OF THE AURORAL EMISSION INTENSITIES WITH THE CHARACTERISTICS OF PRECIPITATING ELECTRONS

In future an orbital experiments [8] is planned to obtain distributions of emission intensities at $\lambda 630.0$ [OI], $\lambda 427.8$ (N_2^+), and $\lambda 486.1$ (H_β) nm within the field-of-view angle $2\omega = 30^\circ$ (three coaxial channels in an auroral imager directed in the nadir with synchronous exposition times of images). We will construct maps of emission intensities and of their ratio $I(630.0)/I(427.8)$ that depend on the altitude h and are functionally related to the average electron energy E_{av}^e normalized by the unit energy flux F_e for the Maxwell spectrum [3]. Figure 1 shows the dependences of the ratios of the emission intensities $I(630.0)/I(427.8)$ and $I(557.7)/I(427.8)$ on the altitude h above the Earth's surface. The relationship between the ratio of the emission intensity $I(427.8)$ to the energy flux F_e of precipitating electrons and the average energy derived in [4] in the form

$$I(630.0)/I(427.8) = 10^{1.3-8\cdot10^{-5}(260-h)^2-4\cdot10^{-7}(260-h)^3}, \quad (1)$$

$$I(630.0)/I(427.8) = 6.6\cdot E_{\text{av}}^{-2.1}, \quad (2)$$

$$I(557.7)/I(427.8) = 10^{1.1-10^{-4}(200-h)^2}, \quad (3)$$

$$I(557.7/427.8) = 11.2\cdot E_{\text{av}}^{-0.3} \quad (4)$$

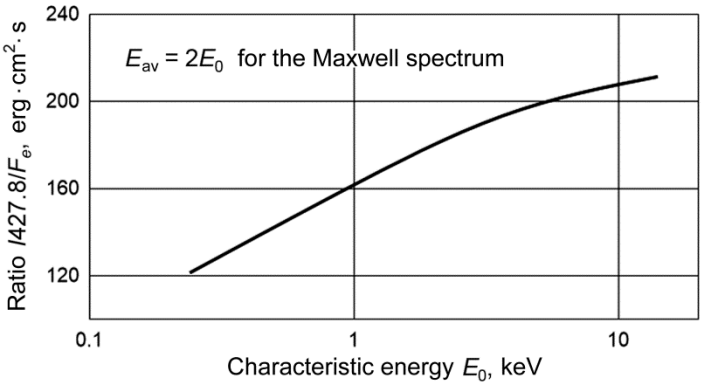

Fig. 2. Dependence of the ratio of the intensity of emission $\lambda 427.8$ to the energy flux of precipitating electrons F_e on the characteristic energy E_0 of precipitating electrons [4].

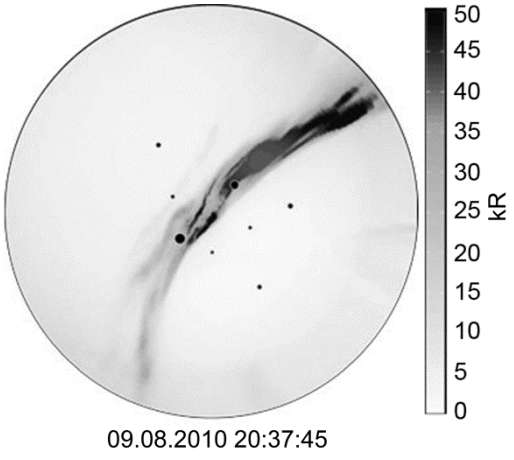

Fig. 3

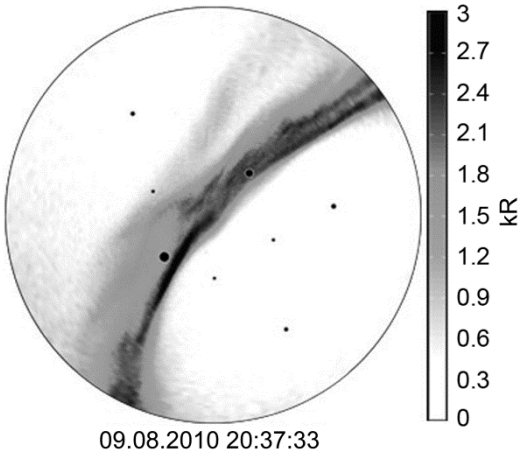

Fig. 4

Fig. 3. Example of all-sky-image of $I(557.7)$ nm at an altitude of 120 km recorded at the Amundsen–Scott Station [9].

Fig. 4. The same as in Fig. 3, but for $I(630.0)$ nm at an altitude of 200 km.

is shown in Fig. 2.

One of the purposes of the future experiment on the SV Meteor-MP is investigation of the influence of the energy characteristics of precipitating electrons on the propagation of signals from navigation systems passing through auroral structures. Taking into account that the altitude of emissions N_2^+ ($\lambda 427.8$ nm) h = 100 km is close to the altitude of oxygen emission $\lambda 557.7$ ($h \approx 115-120$ km) (Fig. 4 in [8]) observed at the Amundsen–Scott Station, we decided to test how the magnetic conjugation of geometrically *coaxial* image fragments of auroral imager affects the spatial distribution and the ratio of the intensities on the example of the ratio $I(630.0)/I(557.7)$ that also depends on the altitude h and is functionally related to E_{av}^e (see Eq. (4) for the Maxwell spectrum [4]).

In the first stage of work, scaling and combination was performed of four pairs of all-sky-images (images of the entire hemisphere) of auroral emissions $\lambda 557.7$ and $\lambda 630.0$ nm (Figs. 3 and 4) observed in August, 2010 at the

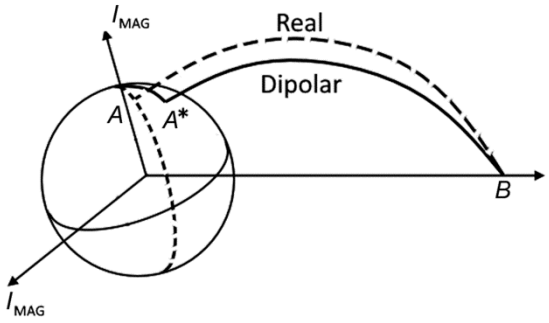

Fig. 5. Determination of the corrected geomagnetic coordinates (CGM).

Amundsen–Scott Station at altitudes of 120 and 200 km, respectively, and presented in artificial colors in [9]. The closed circles indicate places where GPS signals passed through auroral structures and in which phase scintillations were observed (the circle diameter depends on the value of the scintillation index) at time moments close to the exposure time.

On the right of Figs. 3 and 4, absolute emission intensities, in kR, are shown. The algorithm of identification of fragments in all-sky-images was described in [9] and is not presented in this work.

2. RATIO OF THE INTENSITIES FOR EACH FRAGMENT OF EMISSION IMAGES

The sizes of each image shown in Figs. 3 and 4 were 586 × 586 pixels. They were oriented so that the positive direction of the ordinate pointed to the Greenwich meridian. Using the properties discussed above and assuming that the center of images coincides with the coordinates of the Amundsen-Scott Station $(-90^\circ, 0^\circ)$, the ratio of the intensities of two emissions can be calculated. Preliminary, the images must be rotated through the delay angle that arises because of the Earth rotation during the preset time interval because of different expose times of the images. To take advantage of the geometrical method of imposition of two images, it is necessary to execute the following actions:

1) to determine the coordinates of each fragment relative to the image center (the coordinates of the Amundsen–Scott Station) of the celestial sphere;

2) knowing the number of pixels in the image and the physical size of the photograph of the celestial sphere in kilometers, to calculate the coordinates of each fragment relative to the geocenter;

3) then to go back from the geocentric coordinates to pixels, we must find the difference between the coordinates of the Station and the obtained geocentric coordinates of the image fragments;

4) to repeat items 2 and 1 in the reverse order.

However, because of the deviation from the normal and the curvature of the m.f.l., the ratio of the emission intensities at different altitudes must be calculated for the magnetically conjugate image fragments. Therefore, additional actions between steps 2 and 3 are executed:

a) transition to the geomagnetic system of coordinates;

b) tracing along the geomagnetic field line from each fragment of the image $\lambda 630.0$ nm to the image of the fragment $\lambda 557.7$ nm.

The procedure of tracing along the geomagnetic field line, constructed by N. A. Tsyganenko [11] based on the IGRF NASA model of the geomagnetic field and using the software package GEOPACK-2008 consists of the following steps: the initial coordinates are traced along the magnetic field line from the preset altitude to the magnetic equatorial plane with allowance for all nondipolar harmonics in the main field, then reverse tracing to the required altitude, but already with the use of only the dipolar model of the external field. Exactly point *A** to which the procedure of tracing is returned will be the CGC for point *A* from which we started (Fig. 5).

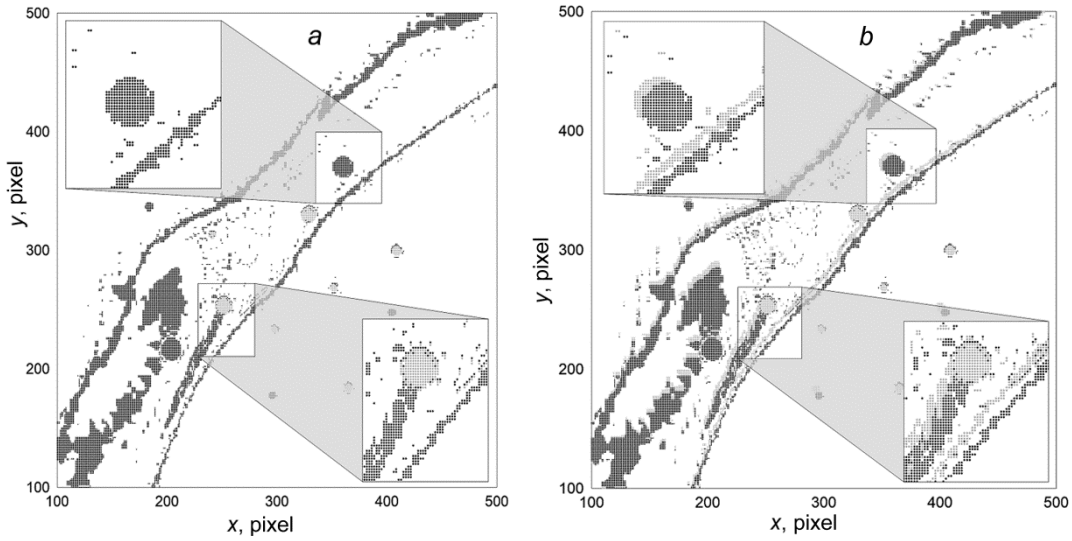

Fig. 6. Displacement of images of emissions at different altitudes conjugated by: *a*) geometrical imposition (along the observation vectors of each fragment) of two images and *b*) by the magnetic field of the image fragments. Rectangles indicate magnified image fragments in which displacements of the intensities are the most pronounced.

Figure 6 illustrates displacements of pixels of images of emissions at altitudes of 120 km (grey color) and 200 km (black color), respectively, conjugated by geometrical imposition of two images (*a*) and by magnetic field of the image fragments (*b*). Rectangles indicate regions in which the displacements of the intensities were more pronounced. From Fig. 6*a* it can be seen that the geometrical method of imposition of two images at different altitudes does not provide the complete pattern of geomagnetic field change depending on the altitude. However, the application of the method of tracing along the field line between the two altitudes (Fig. 6*b*) allows the displacement of scintillations by several image fragments to be seen that corresponds to distances of ~30 km.

Figure 7 shows the map of the ratio of the intensities of emissions at different altitudes conjugated along the observation vectors of each image fragment. To the right of Fig. 7*a*, the black-and-white scale of the ratio of the intensities $I(557.7)$ nm and $I(630.0)$ nm is shown whose values do not exceed 1.6.

3. ANALYSIS OF NUMERICAL RESULTS

In the course of image processing (Figs. 3 and 4), the following results were obtained:

1) Images of emissions at altitudes of 120 and 200 km (Fig. 6) conjugated by the geometrical imposition of the two images and by the magnetic field lines were constructed. After imposition of images on each other, it is seen that after the tracing procedure the fragments are displaced along the axes (Fig. 6*b*). The displacement along the *x* axis was ~4 pixels, and along the *y* axis it was ~6 pixels, which corresponded to ~22.2 and 33.3 km, respectively. Such distances can be commensurable and can even considerably exceed the minimal transverse size of the auroral structures and *dark* intervals between them [7].

2) Maps of the ratio of the intensities of emissions $I(630.0)/I(557.7)$ nm were constructed (Fig. 7) conjugated along the observation vectors of each image fragment. As can be seen from the white-black color scale to the right of Fig. 7*a*, the most part of values of the intensity ratio is of grey color and hence does not exceed 0.5. As expected, the magnetic conjugation of emissions at different altitudes changes the spatial pattern of the ratio of the intensities of emissions at different altitudes in comparison with that obtained by their geometrical conjugation.

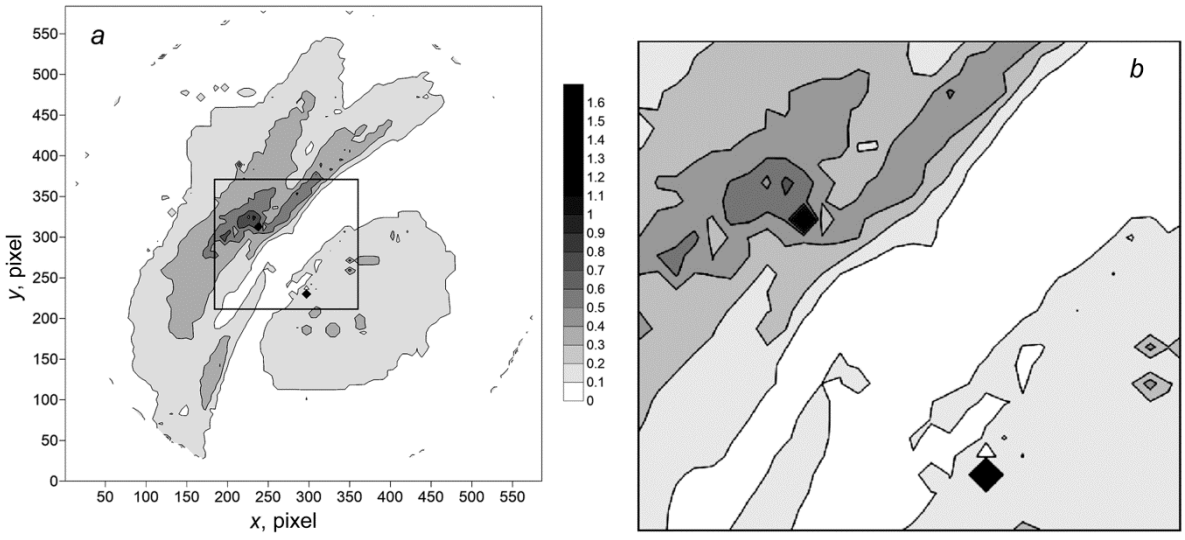

Fig. 7. Map of the ratio $I(630.0)/I(557.7)$ of the intensities of emissions at different altitudes (*a*) conjugated along the observation vectors of each fragment (for Fig. 3) and magnified fragment of the black rectangle shown in Fig. (*a*).

3) According to [2], as a consequence of the displacement, the spatial distributions of the average electron energy (functionally related to the ratio of the intensity of emissions (see Eq. (2)) normalized by the unit flux of the electron energy F_e) changes at least by several tens of electronvolts in comparison with the distribution E^e_{av} calculated from the ratio of the intensities of emissions taken with their geometrical conjugation. A more exact value of change of E^e_{av} could be judged in the presence of experimental data on F_e. The distribution of $I(427.8)$ nm on the basis of which it will be possible to determine F_e (see Fig. 2) are planned to be measured in future experiment with Aurovizor-VIS/MP imager; in addition, the form of the electron energy distribution will be directly measured from onboard the SV Meteor-MP. Nevertheless, from the above examples of the ground-based images recorded above the South Pole it is clear that the difference in the average energies of precipitating electrons determined by the remote method from an orbit taking into account tracing along the m.f.l. can significantly affect the knowledge of the conditions of signal propagation in a local region of the polar ionosphere and finally, the ascertaining of the dependence of changes of the phase scintillation index when the signal intersects the auroral structures of different scales.

CONCLUSIONS

The magnetic conjugation of fragments of images of emissions at different altitudes has refined the spatial picture of the ratio of the intensities of emissions at different altitudes compared to that obtained by geometrical imposition along the parallel observation vectors that finally leads to significant refinement of E^e_{av} calculated from the ratio of emission intensities.

The examined technique of analysis will allow the position of concrete fragments of images of emissions at different altitudes to be refined by their magnetic conjugation with the position of the SV center of mass in the vicinity of which the energy characteristics F_e and E^e_{av} of precipitating particles are measured and the energy characteristics of precipitating particles reconstructed by solving the inverse problem for all observed emissions to be remotely (from an orbit) mapped more correctly. The energy characteristics of particles measured directly onboard the SV Meteor-MP will be compared (by solving the direct problem) with the characteristics obtained remotely at the point located under the magnetic field line whose position will be calculated for each image of auroral emissions at the corresponding

altitudes. This, in turn, will positively affect the accuracy of detailed correlation analysis of positions of ionospheric scintillations with distributions of E_{av}^{e} of precipitating electrons, their energy flux, gradients N_e formed in the region of the ionospheric *E*-layer maximum, and gradients of the transverse conductance of the ionosphere calculated based on the images of auroral emissions. We are sure that the above-described technique of refinement of spatial distributions of the average electron energy determined remotely by the optical method will allow us in future to ascertain the cause and effect relationships of scintillations of radio signals passing through auroral structures.

This work was supported in part by the President of the Russian Federation (scholarship to young scientists and post-graduate students SP-4301.2016.5-SP-2016).

REFERENCES

1. G. Gustafsson, N. E. Papitashvili, and V. O. Papitashvili, J. Atmos. Terr. Phys., **54**, Nos. 11/12, 1609–1631 (1992).
2. P. Janhunen, J. Geophys. Res., **101**, No. A9, 18505–18516 (2001).
3. D. P. Steel and D. J. McEwen, J. Geophys. Res., **95**, No. A7, 10321–10336 (1990).
4. M. H. Rees and D. Luckey, J. Geophys. Res., **79**, No. 4, 5181–5186 (1974).
5. B. V. Kozelov, V. E. Ivanov, and T. I. Sergienko, Geomagn. Aeronom., **42**, No. 4, 513–518 (2002).
6. Zh. V. Dashkevich, V. E. Ivanov, and B. Z. Khudukon, Ann. Geophys., **25**, 1131–1139 (2007).
7. A. K. Kuzmin, Preprint Pr-2161, Space Research Institute of the Russian Academy of Sciences (2011); http://new.cosmos.ru/sites/default/files/books/ 2011kuzmin.pdf.
8. A. K. Kuzmin, M. A. Banshchikova, Yu. S. Dobrolenskii, *et al*., in: Practical Aspects of Geliogeophysics, Collection of Papers, Publishing House of the Space Research Institute of the Russian Academy of Sciences (2016), pp. 114–133; http://iki.cosmos.ru/books/2016gelioph.pdf.
9. J. Kinrade, C. N. Mitchell, N. D. Smith, *et al*., J. Geophys. Res.: Space Phys., **118**, 2490–2502 (2013).
10. M. A. Banshchikova, I. N. Chuvashov, and A. K. Kuzmin, Izv. Vyssh. Uchebn. Zaved. Fiz., **56**, No. 10/2, 174–180 (2013).
11. http://geo.phys.spbu.ru/~tsyganenko/Geopack-2008.html.